Support Reconstruction of Dielectric and Metallic Targets via the Contraction Integral Equation

Martina Teresa Bevacqua, *Member, IEEE*, and Tommaso Isernia, *Fellow, IEEE*

***Abstract*— A new method for support reconstruction is proposed based on the contraction integral equation, a smart rewriting of the scattering equations introduced to alleviate the nonlinearity of the inverse scattering problem. Within such a model, in the case of strong and/or metallic targets, or by a suitable choice of a hyperparameter, the inherent auxiliary function encoding the target properties is expected to assume values close to one inside the target and zero outside. Hence, its retrieval, which is achieved herein using a contrast source inversion method, allows the reconstruction of the support of the obstacle at hand. The achievable performance is tested against simulated and experimental data, including nonconvex dielectric and metallic targets. The cases of multifrequency inversion and dispersive targets are also addressed.**

***Index Terms*— Dielectric and metallic targets, inverse problem, inverse scattering problem, microwave imaging, support reconstruction.**

I. Introduction

IN INVERSE scattering problems, one of the main difficulties to be addressed is the nonlinearity [1], [2], [3], which arises from mutual interactions (and self-interactions) among the different parts of the same target. A generalized solution to inverse scattering problems is usually looked for by minimizing a suitable cost function. However, due to the nonlinearity of the underlying problem, this cost function is nonquadratic, so may have many local minima, which are "false solutions" to the problem [4].

Many strategies have been introduced in the literature to defeat nonlinearity. Among them, linearized or anyway approximated models [5], [6], [7] and qualitative methods [8], [9], [10] allow for straightforward implementation and require a limited amount of computer memory and computational time. On the other side, they suffer from several limitations induced by the adopted approximate model or by the inherent physical meaning, respectively. Some examples of approximate methods are Born [5], Rytov [6], and the quadratic model [7], while the most popular method for qualitative support reconstruction is the linear sampling method (LSM) [9].

On the other hand, a possible key to accurate reconstructions is to conveniently rewrite the Lippman–Schwinger basic equation in such a way as to reduce the "degree of nonlinearity" of the relevant inverse scattering problem. Unlike linearized and approximated methods, this strategy does not involve any approximation of the scattering model [11]. Some examples of smart rewriting of the relevant equations are the very recent "Y0" model [12] and the family of integral formulations known as the "new integral equation" (NIE) or even as the "contraction integral equation" (CIE)[1] [13], [14], [15], [16], [17]. All of them, as well as the Strong Permittivity Fluctuation Theory [18], rely on auxiliary functions embedding the target properties and the related use of new integral operators modeling the self and mutual interactions.

A comparison and possible hybridizations of some of the above models have been discussed in [11]. In particular, herein the "degree of nonlinearity" [19] of the CIE model has been shown to be low (with respect to other more traditional formulations) in the case of "strong" scatterers, or anyway by exploiting a large value for a hyperparameter. Then, the corresponding equations can be safely solved in terms of the auxiliary function embedding the target properties. Conversely, a price is paid for increased difficulty in the final mapping from the modified contrast function to the actual physical properties. In fact, strong scatterers (or a large value of the hyperparameter) imply an approximately binary behavior of the auxiliary variable, and it is obviously hard to extract a generically varying function, such as the usual contrast function, from an essentially binary one.

In this article, the above-mentioned interesting features of the CIE model are exploited to solve the corresponding inverse obstacle scattering problem (i.e., retrieving the support of

Manuscript received 10 May 2023; revised 27 November 2023; accepted 4 January 2024. Date of publication 30 January 2024; date of current version 7 March 2024. This work was supported in part by the Next Generation EU–Italian National Recovery and Resilience Plan (NRRP), Mission 4, Component 2, Investment 1.5, call for the creation and strengthening of "Innovation Ecosystems," building "Territorial Research and Development Leaders"(Directorial Decree: 2021/3277) through Project Tech4You–"Technologies for climate change adaptation and quality of life improvement" under Grant CUP C33C22000290006 and Grant ECS_00000009; and in part by the Next Generation EU–Italian NRRP through the partnership on "Telecommunications of the future" through Program "RESTART" under Grant CUP C37G22000480001 and Grant PE00000001. *(Corresponding author: Martina Teresa Bevacqua.)*

Martina Teresa Bevacqua is with the Department of Ingegneria dell'Informazione, delle Infrastrutture e dell'Energia Sostenibile (DIIES), Università Mediterranea di Reggio Calabria, 89124 Reggio Calabria, Italy, also with the Consorzio Nazionale Interuniversitario per le Telecomunicazioni (CNIT), 43124 Parma, Italy, and also with the Inter-University National Research Center on Interactions between Electromagnetic Fields and Biosystems (ICEmB), 16145 Genoa, Italy (e-mail: martina.bevacqua@unirc.it).

Tommaso Isernia is with the Department of Ingegneria dell'Informazione, delle Infrastrutture e dell'Energia Sostenibile (DIIES), Università Mediterranea di Reggio Calabria, 89124 Reggio Calabria, Italy, also with the Consorzio Nazionale Interuniversitario per le Telecomunicazioni (CNIT), 43124 Parma, Italy, also with the Inter-University National Research Center on Interactions between Electromagnetic Fields and Biosystems (ICEmB), 16145 Genoa, Italy, and also with IREA-CNR, 80124 Naples, Italy (e-mail: tommaso.isernia@unirc.it).

Color versions of one or more figures in this article are available at https://doi.org/10.1109/TAP.2024.3353314.

Digital Object Identifier 10.1109/TAP.2024.3353314

[1]Although in the previous papers from the same authors the acronym NIE was used, in the following, the relevant model is referred to as the CIE model.

the unknown targets) rather than pretending to retrieve the electromagnetic parameters. While being (obviously) related to the previous work wherein CIE has been introduced [13], this article is not a simple extension. Indeed, in [13], a moderate value of the relevant hyperparameter β is actually used to avoid an approximately binary behavior of the auxiliary variable, which would imply significant difficulties in extracting the actual electromagnetic properties of the target. This consideration, completely missing in [13], is instead conveniently noticed and herein valorized for a different scope and also in the case of multifrequency inversions and dispersive targets. As no approximation is involved and the formulation remains nonlinear, the approach is also very different from linearized or qualitative approaches [5], [6], [7], [8], [9], [10].

This article is organized as follows. The inverse scattering problem is formulated in Section II, while in Section III, the CIE model is briefly recalled. Section IV outlines the new proposed procedure, wherein the contrast source inversion (CSI) scheme is adopted [20] for both cases of single and multiple frequencies. In Sections V and VI, we assess the capabilities of the new procedure against both numerical and experimental data, showing that it outperforms the standard qualitative LSM in the case of nonconvex targets. Finally, conclusions follow.

Throughout this article, we consider the canonical 2-D scalar problem (TM polarized fields) and linear media and assume and drop the time-harmonic factor $exp\{j\omega t\}$.

II. Mathematical Formulation of the Problem

For each scattering experiment, the (inverse) scattering problem can be described using two integral equations: the data and the state equations. The first one relates the collected scattered field E_s to the contrast sources W, while the state equation, also known as the Lippman–Schwinger equation, expresses the contrast sources W in terms of the incident field E_i and the contrast function χ encoding the target properties.

In the case of a 2-D scenario with a TM polarized field and a given frequency f, the two equations read as follows [1], [2], [3]:

$$\begin{aligned} E_s(\underline{r}_m, \underline{r}_t, f) &= \int_D G_b(\underline{r}_m, \underline{r}', f)\chi(\underline{r}', f)E_t(\underline{r}', \underline{r}_t, f)dr' \\ &= A_e\big[W(\underline{r}, \underline{r}_t, f)\big] \end{aligned} \tag{1}$$

and

$$\begin{aligned} &W(\underline{r}, \underline{r}_t, f) \\ &\quad = \chi(\underline{r}, f)E_i(\underline{r}, \underline{r}_t, f) \\ &\qquad + \chi(\underline{r}, f)\int_D G_b(\underline{r}, \underline{r}', f)\chi(\underline{r}', f)E_t(\underline{r}', \underline{r}_t, f)dr' \\ &\quad = \chi(\underline{r}, f)E_i(\underline{r}, \underline{r}_t, f) + \chi(\underline{r}, f)A_i\big[W(\underline{r}, \underline{r}_t, f)\big] \end{aligned} \tag{2}$$

where $\underline{r}$ scans the investigation domain D and $\underline{r}_m$ and $\underline{r}_t$ are, respectively, the positions of the receiving and transmitting antennas,[2] located on a given curve Γ, exploited to perform the scattering experiments. $G_b(\underline{r}, \underline{r}', f)$ is the Green's function pertaining to the background medium having complex permittivity ϵ_b. A_e and A_i are short notations of the external and internal radiation operators, respectively. Finally, $\chi(\underline{r}, f) = \epsilon_s(\underline{r}, f)/\epsilon_b - 1$ relates the unknown complex permittivity ϵ_s of the scatterers embedded in the investigation domain D to that of the host medium ϵ_b.

In the following, (1) and (2) are denoted as the H0 model. Notably, as χ depends on the frequency, possibly dispersive obstacles are here considered.

As extensively discussed in [19], the difficulty of the inverse problem of recovering χ is intimately related to the norm of the operator χA_i. In fact, the lower such a value, the closer the problem is to a linear one. Then, the value of such a norm can be considered a measure of the "degree of nonlinearity" of the problem [19]. Also note that an estimation (actually, an upper bound) of such a norm can be given by separately looking at the norms of A_i and χ [19].

III. CIE Model

Problems (1) and (2) are unfortunately nonlinear, as the contrast sources W also depend on the unknown of the problem χ. Moreover, it is also ill-posed due to the properties of the integral radiation operator A_e [1], [2], [3].

To circumvent the difficulties arising from nonlinearity, the CIE model rewrites differently the standard state equation (2) by introducing a new auxiliary unknown R encoding the target properties [11], [13].

In the CIE model, the state equation is rewritten as follows:

$$\begin{aligned} W^{CIE}(\underline{r}, \underline{r}_t, f) &= R(\underline{r}, f)E_i(\underline{r}, \underline{r}_t, f) \\ &\quad + R(\underline{r}, f)A_i^{CIE}\big[W^{CIE}(\underline{r}', \underline{r}_t, f)\big] \end{aligned} \tag{3}$$

wherein

$$R(\underline{r}, f) = \frac{\beta\chi(\underline{r}, f)}{\beta\chi(\underline{r}, f) + 1} \tag{3.a}$$

is the modified contrast function and β is a hyperparameter such that the denominator of $R(\underline{r})$ is different from zero, and assumed herein to be real, positive, and constant [13]. Finally

$$W^{CIE}(\underline{r}, \underline{r}_t, f) = \beta W(\underline{r}, \underline{r}_t, f) \tag{3.b}$$

$$A_i^{CIE}[\cdot] = I + \frac{1}{\beta}\int_D G_b(\underline{r}, \underline{r}', f)[\cdot]d\underline{r}'. \tag{3.c}$$

In the following, (1) and (3) are referred to as the CIE model.

With respect to (2), (3) has the same structure, where the integral internal operator is substituted by A_i^{CIE}, while the contrast sources and the function χ are now replaced by βW and R, respectively.

It follows that the degree of nonlinearity in the inverse problem of recovering R from (1) and (3) is now related to the norm of RA_i^{CIE}. This latter can be estimated and compared to χA_i by separately considering the norm of R and the norm of A_i^{CIE} [11]. When the norm of RA_i^{CIE} is lower than the one of χA_i, the CIE model is expected to be more convenient with respect to the H0 model.

IV. Support Retrieval via the CIE Model

A. Discerning Some Interesting Properties of the Auxiliary Variable R

Given the fact that the norm of a compound operator is bounded by the product of the norms of the operators at hand,

[2]Herein, for the sake of simplicity, they are modeled as elementary sources and ideal probes.

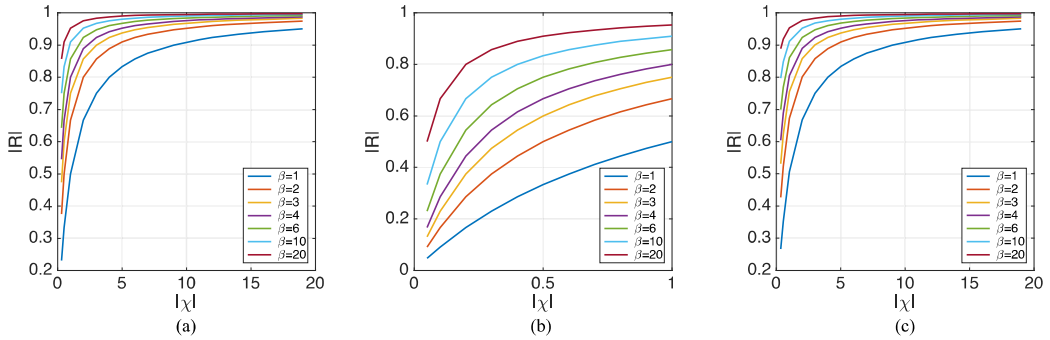

Fig. 1. (a) Norm of the auxiliary contrast function R versus the norm of the contrast function χ in the case of no losses. (b) Zoomed-in view of the portion $|\chi| < 1$ of the curves displayed in (a). (c) Norm of the auxiliary contrast function R versus the norm of the lossy contrast function χ, in the case of electrical conductivity equal to 0.01.

it makes sense to compare the norms of the different operators entering the state equations for both formulations (1) and (2) and (1) and (3).

In the case of large β, the norm of A_i^{CIE} approaches the unitary value. Indeed, a larger value for β allows the local effect of the current to overcome the global one [13]. Hence, in the case of large contrasts and/or large scatterers, provided the value of β is sufficiently large, the norm of A_i^{CIE} is smaller than the one pertaining to A_i (see [11] for more details).

It also makes sense to compare the norm of R with the norm of χ. To this end, an analytical discussion is reported in the Appendix, wherein it is shown that if $0 < \beta < 1$, in the first and fourth quarters of the plane $\chi_r \chi_i$, the norm of R is always lower than the norm of χ. Instead, when the hyperparameter β is increasing, the norm of R is higher than the one of χ if $|\chi| < 1$. If $|\chi| > 1$, the norm of R is instead lower than the one of χ and the CIE model can be convenient with respect to the H0 model.

For the sake of simplicity, in Fig. 1(a) and (b), the norm of the auxiliary function R versus the one of the contrast function χ is reported for the case of lossless, homogeneous background and positive χ [11]. The case of a lossy contrast is instead reported in Fig. 1(c). As can be seen, for increasing values of χ, the norm of R is lower than the norm of χ and asymptotically tends to 1. Also note that in the case of $\chi < (\beta - 1)/\beta$, the norm of R is higher than the one of χ, as can be observed in Fig. 1(b) (see also the Appendix).

As a consequence of all the above (including the comments on the norms of the radiation operators A_i^{CIE} and A_i), the CIE formulation turns out to be more convenient than the H0 model as far as the recovery of the corresponding unknowns is concerned, provided $\beta\chi$ is sufficiently large. On the other side, in the case of very large β, one has an ill-conditioned relationship in the mapping from the modified contrast function R to the physical contrast χ.

While the quantitative inversion procedure in [13] has been based on moderate values of β (usually lower than 6), with the aim of recovering the contrast function, here the idea is to operate with large β to exploit the function R as a support indicator. In fact, apart from a restricted "transition region," whose extension is smaller and smaller for increasing values of the hyperparameter β, R either assumes the value zero (in the regions where there is no scatterer) or is very close to the unitary value (inside the target). Very interestingly, this binary kind of behavior holds true whatever the frequency, so that R becomes poorly dependent on frequency. This circumstance allows for multifrequency inversion without the need to adopt a suitable dispersion relationship, as would be the case with the more standard H0 formulation.

To show some examples, the spatial distributions of R and χ are shown for two different profiles and values of β. As can be seen in Fig. 2, in the cases of strong scatterers (as the brain phantom), also a lower value of β allows us to obtain a binary R function.

It is important to note that in the case of metallic targets, the electrical conductivity of the targets is very large and dominates the relative permittivity. Then, even if β is very low, the corresponding variable R tends to have a unitary value inside the targets. This holds true also in the case of very strong dielectric targets.

B. Support Retrieval Within a CSI Scheme

In the following, the CSI method [20] is adopted to solve the relevant CIE inverse scattering equations (1) and (3). In this article, such an inversion scheme is referred to as CIE-CSI. Both cases of single- and multiple-frequency data are addressed.

In the case of single-frequency data, the support reconstruction consists in minimizing the following cost functional [20]:

$$\begin{aligned}\Phi_{CIE}(R, W^{CIE}) &= \sum_{t=1}^{T} \frac{\left\| W^{CIE} - RE_i - RA_i^{CIE}\left[W^{CIE}\right]\right\|_{\mathrm{D}}^2}{\|E_i\|_{\mathrm{D}}^2} \\ &\quad + \sum_{t=1}^{T} \frac{\left\| E_s - A_e\left[W^{CIE}/\beta\right]\right\|_{\Gamma}^2}{\|E_s\|_{\Gamma}^2} + \Phi_{\mathrm{P}}(R) \end{aligned} \tag{4}$$

wherein T is the total number of transmitters and Φ_P is an additional regularizing term. In the case of multifrequency data, the support reconstruction consists instead in minimizing

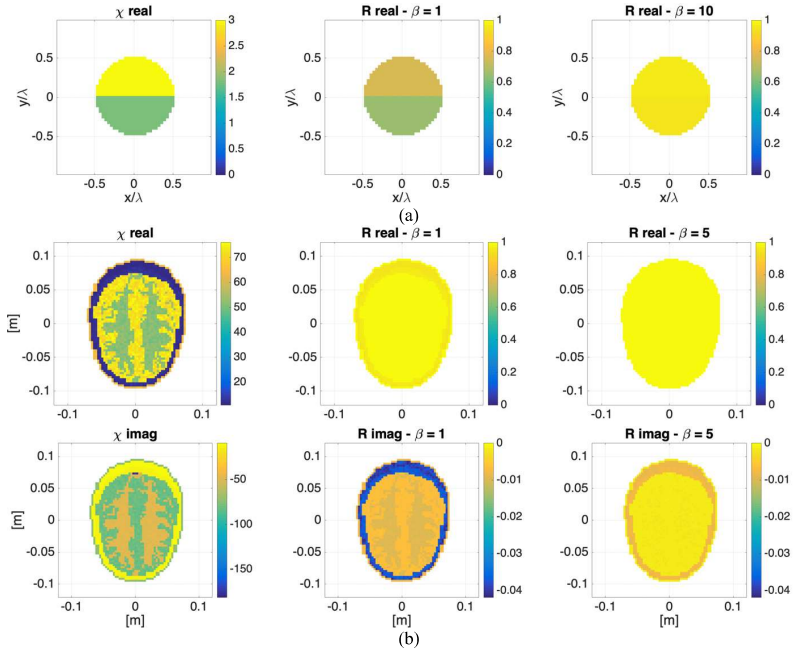

Fig. 2. Spatial distributions of the auxiliary contrast function R versus the original contrast function χ in the case of (a) lossless inhomogeneous cylinder and (b) realistic brain phantom.

the following cost functional [21]:

$$\Phi_{CIE-MF}\left(R, W^{CIE}\right) = \sum_{k,t=1}^{F,T} \frac{\left\| W^{CIE} - RE_i - RA_i^{CIE}\left[W^{CIE}\right]\right\|_{\mathrm{D}}^2}{\|E_i\|_{\mathrm{D}}^2} + \sum_{k,t=1}^{F,T} \frac{\left\|E_s - A_e\left[W^{CIE}/\beta\right]\right\|_{\Gamma}^2}{\|E_s\|_{\Gamma}^2} + \Phi_{\mathrm{P}}(R) \tag{5}$$

wherein F is the total number of frequencies.

It is important to note that, unlike the standard scattering H0 model, in the above cost function, no dispersion relation has to be considered for the auxiliary variable R. Indeed, this latter exhibits an approximatively binary behavior whatever the frequency f.

Further advantages can be taken from the essentially binary behavior of the function R. In fact, inspired by [22], the cost functions (4) and (5) can be equipped using the following penalty term:

$$\Phi_P(R) = \gamma \|R(R-1)\|_D^2 \tag{6}$$

where γ is the nonnegative parameter controlling the relative weight of such a regularization term. This additive term aims to make the punctual values of the unknown function only belong to a given finite alphabet of values of zero or one [22]. It is worth noting that the above penalty term does not modify the computational complexity of our standard approach. In fact, the function is still a fourth-order polynomial in the unknowns, so it can still be efficiently minimized by using a conjugate gradient scheme and exploiting closed-form line minimization steps [22].

C. On the Selection of the β Variable

When no a priori information on the expected e.m. properties of the dielectric target is available, a larger and larger value of β is appropriate. However, in our experience, a larger β is expected to make the ill-conditioning worse. Indeed, in [13], the inversion procedure starts with a large β and a small number $\mathrm{M_F}$ of Fourier bases for the ambiguous part of the induced current, which means that the optimization is carried out in a small current subspace, and a strong regularization is enforced.

On the other hand, when a priori information is available, it is convenient to take it into account. For instance, if both dielectric and metallic targets are present in the region of interest, one can obviously select β depending on the expected e.m. properties of the dielectric target. In fact, whatever β, R associated with the metallic target tends to 1. As far as the dielectric part is concerned, if it is expected to be strong, $\beta = 1$ already allows the binary approximation to be accurate, while in the case of weak targets, a larger β (for instance, 10) must be preferred.

In the following, the hyperparameter β is set to 10 and 1 in the cases of dielectric and metallic targets, respectively. Moreover, in the case of the simultaneous presence of dielectric and metallic targets, an analysis with β equal to 1 and 10 is performed in the following.

V. Numerical Assessment Against Simulated Data and Dielectric Targets

The performance of the proposed method has first been tested against dielectric nonconvex targets and simulated data. For the sake of comparison, the inversions have also been

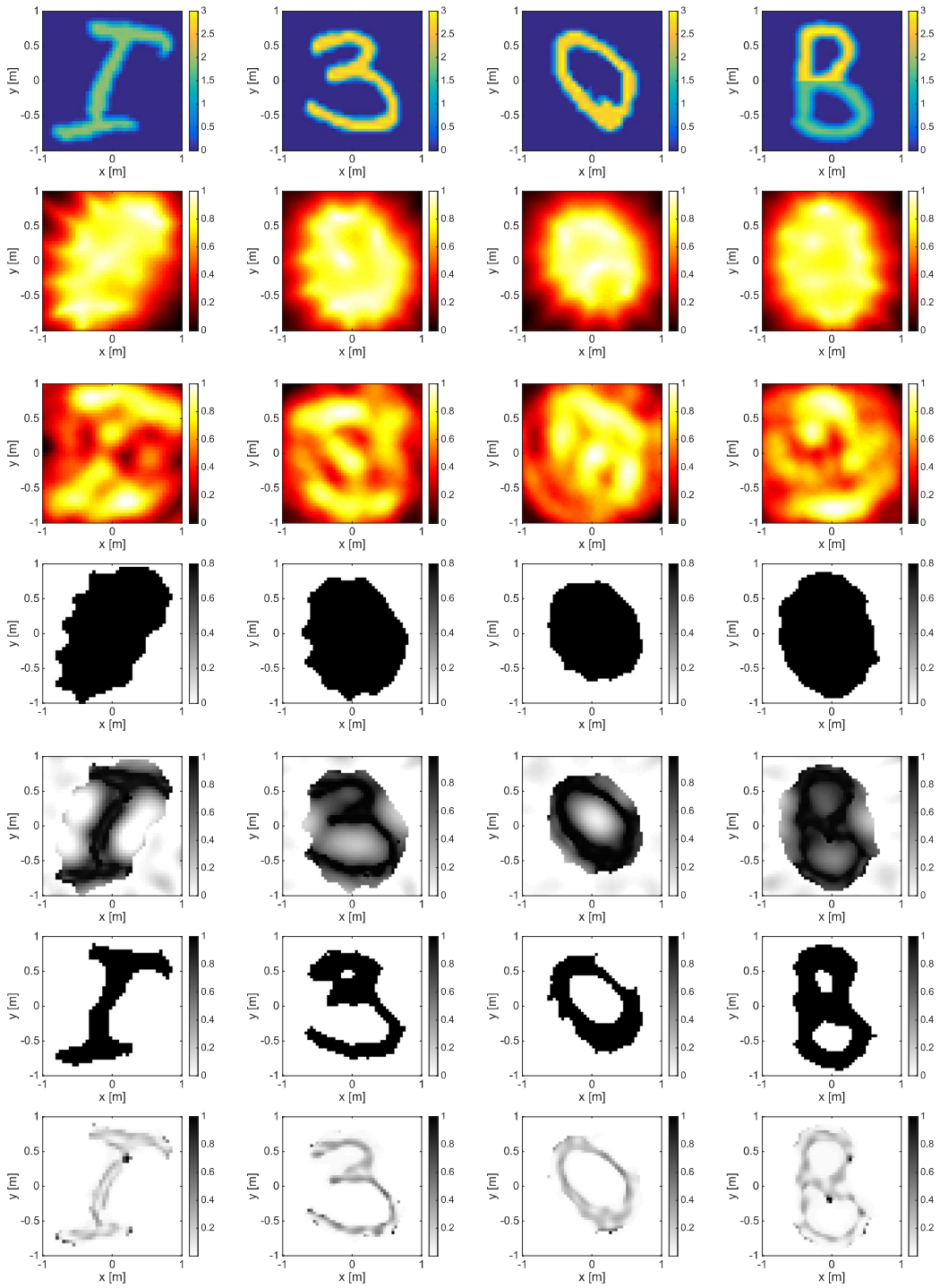

Fig. 3. Single frequency inversion at 300 GHz. From top to bottom: actual χ profile; normalized LSM indicators; normalized OSM indicators; starting guesses of the iterative procedure; retrieved R functions using CIE-CSI and enforcing a lossless profile; binarized maps (70%) of the retrieved R; normalized energies of the retrieved currents W^{CIE}. The I-shaped target has a maximum permittivity $\epsilon_r = 3$ and $N_x = N_y = 42$. The three-shaped and O-shaped targets have a maximum permittivity $\epsilon_r = 4$ and $N_x = N_y = 50$. The two-level B-shaped target with two levels of permittivity $\epsilon_r = 4$, $\epsilon_r = 2.8$, and $N_x = N_y = 50$. (NMSE $= 0.20$, iter $= 1719$, SSIM $= 0.31$, and SSIM $= 0.64$ for the binarized map.) More details about the targets can be found in Table I.

performed by means of a popular and simple qualitative method, namely the LSM [9]. Moreover, the binarized LSM maps have been assumed as a starting guess for the auxiliary function in the optimization procedure underlying CIE-CSI,

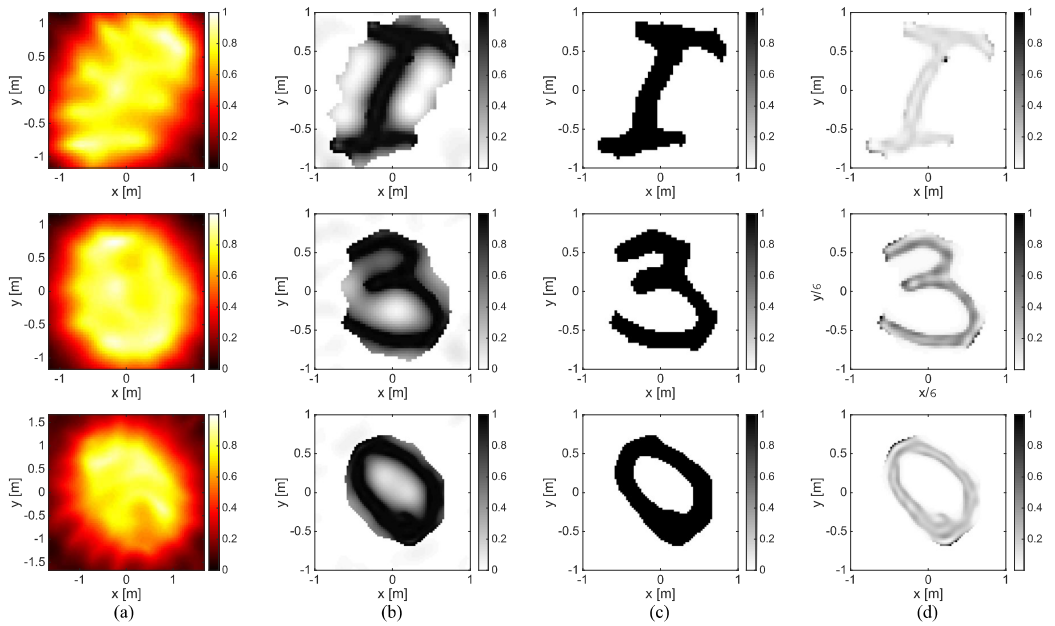

Fig. 4. Multifrequency inversion at [250 300 350] MHz. (a) Normalized multifrequency LSM indicators. (b) Retrieved R using CIE-CSI and enforcing a lossless profile. (c) Binarized maps (70%) of the retrieved R. (d) Normalized energies of the retrieved currents $\mathrm{W}^{\mathrm{CIE}}$. The I-shaped target has a maximum permittivity $\epsilon_r = 3$ and $N_x = N_y = 50$. The three-shaped and O-shaped targets have a maximum permittivity $\epsilon_r = 4$ and $N_x = N_y = 58$.

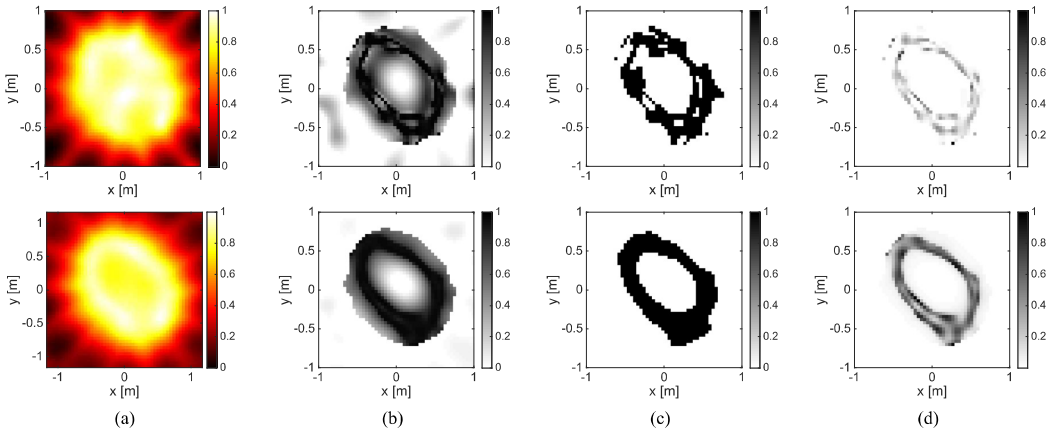

Fig. 5. Inversion with undersampled data. Assessment against an O-shaped target with maximum permittivity $\epsilon_r = 4.2$ and $N_x = N_y = 50$. (a) Normalized LSM indicators (multifrequency in the second row). (b) Retrieved R using CIE-CSI and enforcing a lossless profile. (c) Binarized maps (70%) of the retrieved R. (d) Normalized energies of the retrieved currents $\mathrm{W}^{\mathrm{CIE}}$. First row: single-frequency inversion (NMSE = 0.31, iter = 4699, SSIM = 0.17, and SSIM = 0.6 for the binarized map). Second row: multifrequency at [250 300 350] MHz (NMSE = 0.16, iter = 1379, SSIM = 0.33, and SSIM = 0.75 for the binarized map).

wherein the binarization threshold is chosen to be equal to 0.65. The starting guess for the contrast sources has instead been evaluated as $R_{initial} E_i$.

The dielectric targets, depicted in Figs. 3–6, belong to the MNIST dataset [23], which contains both handwritten numerals and letters. The targets are embedded in a square domain with a side L = 2 m and filled with a medium with the properties of air. Moreover, the domain is discretized into $N_x \times N_y$ small cells, with N_x and N_y being the number of cells along the x and y directions. Each target is probed by means of $N_T = N_R = 20$ receivers and transmitters, modeled as line sources located on a circumference Γ of radius R = 3.75 m. The scattered field data, simulated by means of a full wave in-house forward solver based on MoM, have been corrupted with a random Gaussian noise with an SNR = 30 dB.

The normalized mean square errors between the retrieved auxiliary function $\widetilde{R}$ and the actual one R, defined as

$$NMSE = \frac{\left\| R - \widetilde{R} \right\|_D^2}{\| R \|_D^2} \tag{7}$$

have been evaluated to quantitatively evaluate the obtained performance. Moreover, the structural similarity index measure

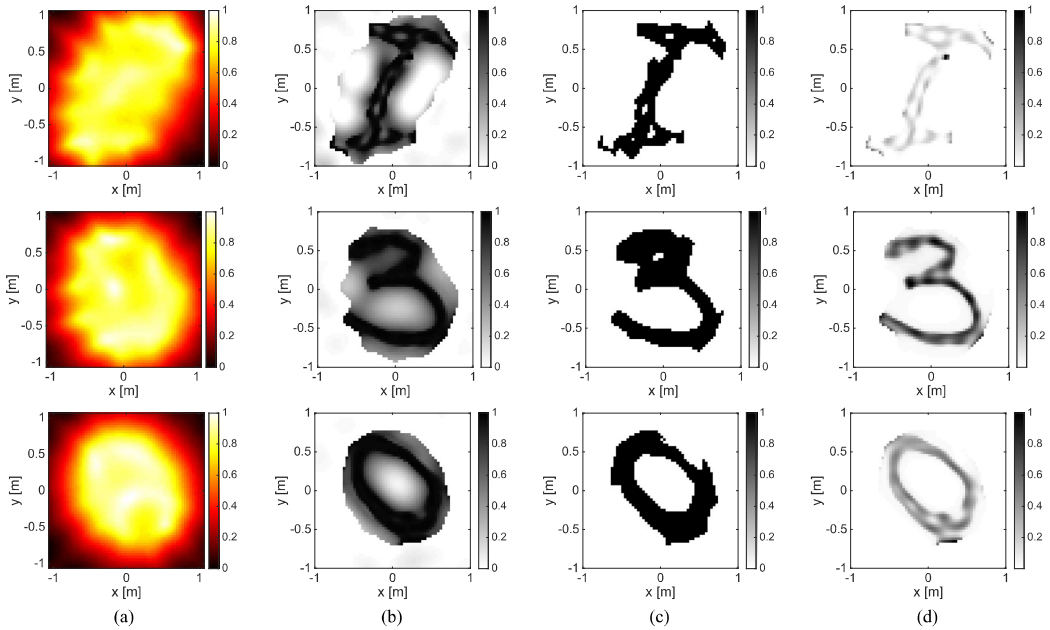

Fig. 6. Multifrequency inversion at [280 290 300 310 320] MHz. Assessment against dispersive targets with maximum permittivity $\epsilon_r = 4.2$ and $N_x = N_y = 60$. (a) Normalized multifrequency LSM indicators. (b) Retrieved R using CIE-CSI and enforcing a lossless profile and a binary penalty term. (c) Binarized maps (70%) of the retrieved R. (d) Normalized energies of the retrieved currents $\mathrm{W}^{\mathrm{CIE}}$.

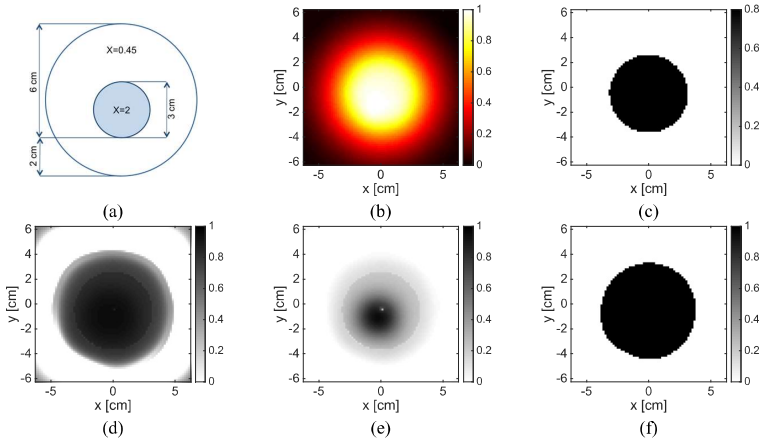

Fig. 7. Experimental dielectric target. Assessment against *FoamDielInt* target at 4 GHz. (a) Sketch of the actual object. (b) Normalized LSM indicator. (c) Starting guess of the iterative procedure. (d) Retrieved R function and (e) energy of the retrieved contrast sources $\mathrm{W}^{\mathrm{CIE}}$ using CIE-CSI and enforcing a lossless profile with positive value. (f) Binarized map (70%) of the retrieved R.

(SSIM) [24] has also been evaluated to measure the similarity between the reconstructed and actual functions.

In Fig. 3, the reconstructions at 300 MHz are shown. In all cases, the LSM is not able to retrieve the actual target support but only their convex hulls. To give additional comparisons, the qualitative maps obtained by means of the orthogonality sampling method (OSM) [10] are reported in Fig. 3. Like the LSM, the OSM is also unable to correctly retrieve the targets.

Differently, by starting from the binarized LSM maps and enforcing only the lossless nature of the variable R, the proposed method can accurately retrieve the target supports. It is important to note that no penalty term has been added to retrieve the support. Interestingly, the supports can also be appreciated in a better fashion by binarizing the retrieved function R (sixth row in Fig. 3) as well as by plotting the energy of the retrieved currents (last row in Fig. 3).

The reconstructions are, as expected, further improved in the case of multifrequency data. In fact, by using a frequency range of 250–350 MHz with a step of 50 MHz, a lower NMSE and a larger SSIM are achieved (see Fig. 4 and Table I).

The capability of the approach to easily deal with multifrequency cases also suggests that one could give up a number of Tx/Rx antennas by using multifrequency data. Then, the case with a number of antennas less than the degrees of freedom

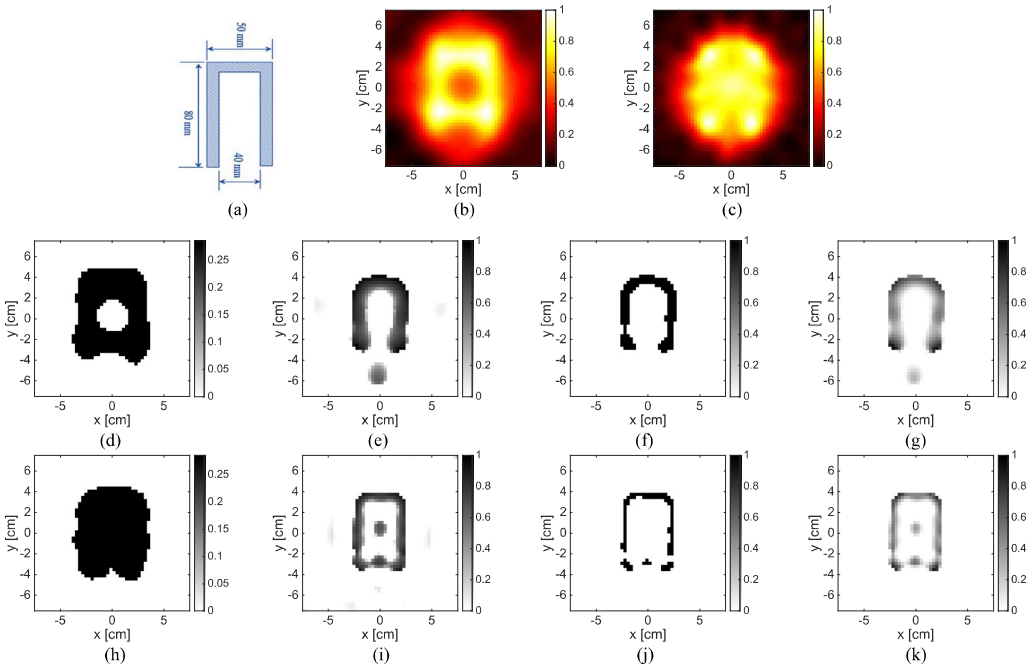

Fig. 8. Experimental metallic target. Assessment against the *U-shaped Fresnel target*: (b) and (d)–(g) at 4 GHz and (c) and (h)–(k) at 6 GHz. (a) Sketch of the actual object. (b) and (c) Normalized LSM indicators. (d) and (h) Starting guesses of the iterative procedure. (e) and (i) Retrieved R functions using CIE-CSI and enforcing a lossless profile with positive value, and a binary penalty term. (f) and (j) Binarized maps (70%) of the retrieved R. (g) and (k) Normalized energy of the retrieved contrast sources W^{CIE}.

of scattered fields ($N_T = N_R = 14$) and three frequencies have been considered. Fig. 5 reports the reconstructions of the O-shaped targets in the cases of single-frequency as well as multifrequency data and reduced numbers of antennas. As can be seen, in the case of multifrequency data, the approach provides a better estimation of the support of the target. A similar tradeoff, by compensating spatial frequency information by means of multifrequency data, can also be expected in the case of aspect-limited measurement configurations.

Finally, Fig. 6 shows the case of multifrequency inversion with dispersive targets. The targets have been simulated by considering five frequencies within the range of [280, 320] MHz and a dispersion law such that an increment of $\Delta\epsilon = 0.05$ of the relative permittivity $\epsilon_r = 4$ is examined for each frequency ($N_T = N_R = 20$). This means that the permittivity ranges from 4 to 4.2. Even if the dispersive nature of the targets is not modeled in the inversion (as a unique spatial variable R is looked for during the inversion), their supports are correctly retrieved by the proposed method, as also confirmed by Table II. Note that in this case the cost functional has also been equipped with the binary penalty term in (6) with $\gamma = (N_x N_y)^{-2}$.

VI. Numerical Assessment Against Experimental Data

In this section, examples against experimental data provided by the Institute Fresnel of Marseille [25], [26], [27], widely adopted to test inverse scattering procedures, are reported. The data are collected under a partially aspect-limited configuration, where primary sources completely surround the targets, but, for each illumination, the measurements are taken only on an angular sector of 240°.

The first target is the *FoamDielIntTM* target, which consists of a piecewise inhomogeneous dielectric target made by two nested, nonconcentric, circular cylinders, where the inner one has a contrast ($\varepsilon = 3 \pm 0.3$) larger than the outer one ($\varepsilon = 1.45$). A schematic sketch is shown in Fig. 7. A 90×36 multiview-multistatic data matrix at 4 GHz has been processed, while the scenario of 0.125×0.125 m^2 has been again discretized into 78×78 cells.

As can be seen in Fig. 7, while the LSM correctly retrieves the position and shape of the target, it underestimates its size. Instead, the proposed approach (with $\beta = 10$) can correctly estimate the diameter of the target. Interestingly, the map of the energy of the currents also allows for the identification of the denser regions of the targets.

The metallic *U-shaped target* from the 2001 Fresnel database has also been considered [25], whose dimensions are 80×50 mm^2. A schematic sketch is shown in Fig. 8. The 36×36 multiview-multistatic data matrix at both 4 and 6 GHz has been processed. The investigated area of 0.15×0.15 m^2 has been discretized into 50×50 cells.

The LSM is again not able to retrieve the target support, as it just identifies the convex hull of the target at 6 GHz and a ring at 4 GHz. On the other hand, the proposed method (with $\beta = 1$), equipped with the binary penalty term in (6) (with $\gamma = (N_x N_y)^{-2}$), can provide a correct guess of the shape.

The last target is the *FoamMetExt* target [27], which consists of a foam cylinder with a diameter d = 80 mm, $\varepsilon_s = 1.45 \pm 0.15$, and a copper tube with a diameter

TABLE I

SYNTHETIC PARAMETERS FOR PERFORMANCE EVALUATION: FIGS. 3 AND 4

Target	Single-frequency				Multi-frequency			
	SSIM		NMSE	# Iter	# Iter	SSIM		NMSE
	$\tilde{R}$	bin $\tilde{R}$				$\tilde{R}$	bin $\tilde{R}$	
I shaped	0.34	0.61	0.18	1617	1234	0.33	0.63	0.15
3 shaped	0.28	0.61	0.25	1630	1405	0.32	0.69	0.22
0 shaped	0.33	0.70	0.22	1455	1452	0.43	0.75	0.16

TABLE II

SYNTHETIC PARAMETERS FOR PERFORMANCE EVALUATION: FIG. 6

Target	Multi-frequency			
	# Iter	SSIM		NMSE
		$\tilde{R}$	bin $\tilde{R}$	
I shaped	2643	0.25	0.54	0.19
3 shaped	1051	0.31	0.64	0.25
0 shaped	1150	0.34	0.70	0.21

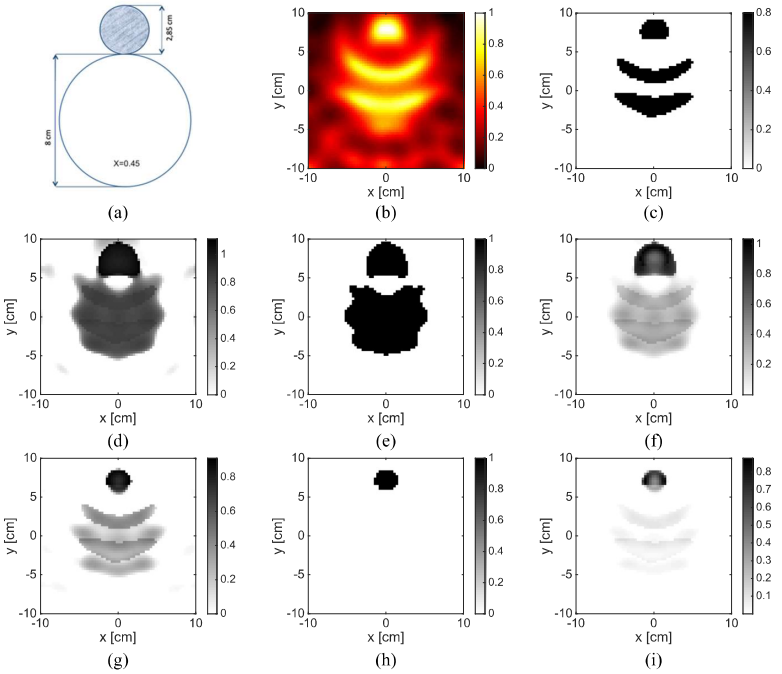

Fig. 9. Experimental metallic and dielectric targets. Assessment against *FoamMetExt* at 4 GHz. (a) Sketch of the actual object. (b) Normalized LSM indicator. (c) Starting guess of the iterative procedure. (d) Retrieved R function using CIE-CSI and enforcing a lossless profile with positive value, and a binary penalty term ($\beta = 10$). (e) Binarized map (70%) of the retrieved R. (f) Normalized energy of the retrieved contrast sources W^{CIE}. (g)–(i) the same as (d)–(f) but for $\beta = 1$.

d = 28.5 mm. The sketch of the target and the reconstructions via the proposed approach are reported in Fig. 9.

To analyze the role of β, two different values are considered. When $\beta = 1$, as $R = 0.31$ inside the foam, the foam region is not completely recovered, and the metallic part is predominant. Instead, when $\beta = 10$, the variable R tends roughly to 0.82 in the foam and is closer to 1. Then, the binary approximation is more effective, and a better reconstruction is obtained. The results agree with the discussion in Section IV-C.

In the above cases in Figs. 7–9, a lossless function R, assuming positive values, has been enforced in the minimization procedure.

VII. CONCLUSION

In this article, the CIE model is exploited to solve the inverse obstacle problem, which gives up the electrical properties of the unknown targets and amounts to retrieving only their supports. Besides the standard minimization procedure, the CIE model involves an additional step to finally retrieve the target contrast function from the auxiliary variable. However, if the target contrast is very large, then the auxiliary variable will have a binary distribution, whatever the working frequency, and it is really complicated to extract the electromagnetic properties from a binary distribution unless a very robust regularization technique is adopted. Then, the proposed method trades the reduction of the achievable

information for the absence of additional steps to retrieve χ from R.

As far as limitations are concerned, it is important to note that, in the case of $|\chi| < 1$, the CIE model may not be convenient with respect to the H0 model. Moreover, the use of a higher hyperparameter β is suggested to obtain R very close to the unitary value. However, in our experience, the higher β, the higher the ill-conditioning and the harder the inversion. To counteract such an issue, a suitable regularization technique is suggested to be adopted. Indeed, besides using CIE-CSI, some regularization strategies have been considered in the numerical section, which enforces some properties on the unknown.

These latter include the use of a proper starting guess, the binary regularization technique as well as some constraints about the absence of losses. Note that the adoption of a proper starting guess is important, especially in the case of higher β as well as larger contrast values. In this article, the normalized LSM maps have been adopted as starting guesses, but other, more convenient, fast qualitative methods can be eventually exploited to gain a first understanding of the unknown target.

The results show that both in cases of metallic and dielectric targets as well as multifrequency and reduced data, the proposed method can improve the support estimation via LSM and accurately retrieve the shapes, emphasizing the corners and the internal coves.

However, with respect to the LSM or other fast qualitative methods, the proposed method is based on the minimization of a nonlinear cost function and hence involves an iterative procedure, which implies a higher computational burden. To give a measure of the required computational cost, we have evaluated the elapsed time for each target in Fig. 3. This time is in the order of a couple of minutes. Note that all the numerical calculations have been run on a personal computer equipped with one Intel i7 (2.5 GHz) processor and 16 GB of RAM.

Limitations are expected with increasing values of the contrast and the extension of the target, but indeed the presented examples show that the approach can outperform existing support estimation techniques. As a matter of fact, starting from a large circular starting guess, a satisfactory retrieval (NMSE $= 0.36$) of the shape of the O-shaped target can be obtained for a value of the relative permittivity as large as 7.

Future work will be devoted to extending and testing the proposed method in 3-D geometry as well as against subsurface and GPR scenarios.

APPENDIX

Let us assume that β is a real, positive constant and different from zero. Under such hypotheses, one can easily investigate when the norm of the auxiliary function R is lower than the norm of the contrast function $\chi = \chi_r - j\chi_i$, that is, $\|R\| < \|\chi\|$. Indeed, the norm can be evaluated as $max|\cdot|$ [11], [19], one can directly compare the absolute values and then consider the following inequality:

$$\frac{|\beta|^2|\chi|^2}{|\beta\chi + 1|^2} < |\chi|^2. \tag{A.1}$$

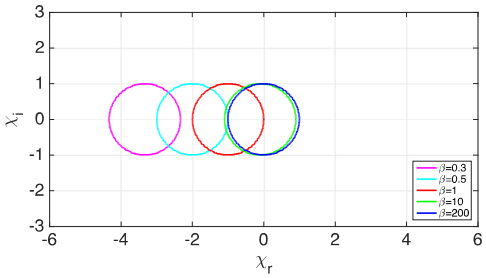

Fig. 10. Contours of the region $\|R\| > \|\chi\|$ in the plane $\chi_r\chi_i$ for different and increasing values of a real, positive constant β. For each β value, the region $\|R\| > \|\chi\|$ is the ones inside the circumference.

By means of further manipulations, the inequality can be simplified as follows:

$$\left(\chi_r + \frac{1}{\beta}\right)^2 + \chi_i^2 > 1. \tag{A.2}$$

The above equation identifies the area outside a circumference of radius 1, and the center $(-(1/\beta), 0)$ in the plane $\chi_r\chi_i$ (see Fig. 10). This means that the norm of the auxiliary variable is always lower than the norm of the contrast function ($\|R\| < \|\chi\|$), excluding a very small region in the neighborhood of the origin of the plane $\chi_r\chi_i$. This is also confirmed by Fig. 1(b). In the case of a real and positive contrast, $\|R\| < \|\chi\|$ any time $\chi > ((\beta - 1)/\beta)$.

If $0 < \beta < 1$, the condition $\|R\| < \|\chi\|$ is always verified in the first and fourth quarters of the plane $\chi_r\chi_i$. Instead, when the hyperparameter β is increasing, the $\|R\| > \|\chi\|$ region tends to be the one corresponding to $|\chi| < 1$. In such a region, the CIE model could not be convenient with respect to the H0 model.

Note that this is just a part of the story, as the norm of A_i^{CIE} has to be checked as well to understand which model is more convenient.

REFERENCES

[1] X. Chen, *Computational Methods for Electromagnetic Inverse Scattering*. Hoboken, NJ, USA: Wiley, 2018.
[2] M. Pastorino, *Microwave Imaging*. New York, NY, USA: Wiley, May 2010.
[3] D. Colton and R. Kress, *Inverse Acoustic and Electromagnetic Scattering Theory*. Berlin, Germany: Springer-Verlag, 1998.
[4] T. Isernia, V. Pascazio, and R. Pierri, "On the local minima in a tomographic imaging technique," *IEEE Trans. Geosci. Remote Sens.*, vol. 39, no. 7, pp. 1596–1607, Jul. 2001.
[5] A. J. Devaney, "Geophysical diffraction tomography," *IEEE Trans. Geosci. Remote Sens.*, vol. GE-22, no. 1, pp. 3–13, Jan. 1984.
[6] A. J. Devaney, "Inverse-scattering theory within the Rytov approximation," *Opt. Lett.*, vol. 6, no. 8, pp. 374–376, 1981.
[7] A. Brancaccio, V. Pascazio, and R. Pierri, "A quadratic model for inverse profiling: The one-dimensional case," *J. Electromagn. Waves Appl.*, vol. 9, nos. 5–6, pp. 673–696, Jan. 1995.
[8] F. Cakoni and D. Colton, *Qualitative methods in inverse scattering Theory*. Berlin, Germany: Springer-Verlag, 2006.
[9] D. Colton and A. Kirsch, "A simple method for solving inverse scattering problems in the resonance region," *Inverse Problems*, vol. 12, no. 4, pp. 383–393, Aug. 1996.
[10] R. Potthast, "A study on orthogonality sampling," *Inverse Problems*, vol. 26, no. 7, Jul. 2010, Art. no. 074015.
[11] M. T. Bevacqua and T. Isernia, "Quantitative non-linear inverse scattering: A wealth of possibilities through smart rewritings of the basic equations," *IEEE Open J. Antennas Propag.*, vol. 2, pp. 335–348, 2021.

[12] M. T. Bevacqua and T. Isernia, "An effective rewriting of the inverse scattering equations via Green's function decomposition," *IEEE Trans. Antennas Propag.*, vol. 69, no. 8, pp. 4883–4893, Aug. 2021, doi: 10.1109/TAP.2021.3060147.

[13] Y. Zhong, M. Lambert, D. Lesselier, and X. Chen, "A new integral equation method to solve highly nonlinear inverse scattering problems," *IEEE Trans. Antennas Propag.*, vol. 64, no. 5, pp. 1788–1799, May 2016.

[14] Y. Zhong and K. Xu, "Contraction integral equation for three-dimensional electromagnetic inverse scattering problems," *J. Imag.*, vol. 5, no. 2, p. 27, Feb. 2019.

[15] Y. Zhong, F. Zardi, M. Salucci, G. Oliveri, and A. Massa, "Multiscaling differential contraction integral method for inverse scattering problems with inhomogeneous media," *IEEE Trans. Microw. Theory Techn.*, vol. 79, no. 1, pp. 4064–4079, Sep. 2023, doi: 10.1109/TMTT.2023.3251573.

[16] D.-M. Yu, X. Ye, X.-M. Pan, and X.-Q. Sheng, "Fourier bases-expansion for three-dimensional electromagnetic inverse scattering problems," *IEEE Geosci. Remote Sens. Lett.*, vol. 19, 2022, Art. no. 5002905.

[17] L. Zhang, K. Xu, Y. Zhong, and K. Agarwal, "Solving phaseless highly nonlinear inverse scattering problems with contraction integral equation for inversion," *IEEE Trans. Comput. Imag.*, vol. 6, pp. 1106–1116, 2020.

[18] J. Ma, W. Cho Chew, C.-C. Lu, and J. Song, "Image reconstruction from TE scattering data using equation of strong permittivity fluctuation," *IEEE Trans. Antennas Propag.*, vol. 48, no. 6, pp. 860–867, Jun. 2000.

[19] O. M. Bucci, N. Cardace, L. Crocco, and T. Isernia, "Degree of nonlinearity and a new solution procedure in scalar two-dimensional inverse scattering problems," *J. Opt. Soc. Amer. A, Opt. Image Sci.*, vol. 18, no. 8, pp. 1832–1843, 2001.

[20] P. M. V. D. Berg and R. E. Kleinman, "A contrast source inversion method," *Inverse Problems*, vol. 13, no. 6, pp. 1607–1620, Dec. 1997.

[21] O. M. Bucci, L. Crocco, T. Isernia, and V. Pascazio, "Inverse scattering problems with multifrequency data: Reconstruction capabilities and solution strategies," *IEEE Trans. Geosci. Remote Sens.*, vol. 38, no. 4, pp. 1749–1756, Jul. 2000.

[22] L. Crocco and T. Isernia, "Inverse scattering with real data: Detecting and imaging homogeneous dielectric objects," *Inverse Problems*, vol. 17, no. 6, pp. 1573–1583, Dec. 2001.

[23] G. Cohen, S. Afshar, J. Tapson, and A. van Schaik, "EMNIST: An extension of MNIST to handwritten letters," 2017, *arXiv:1702.05373*.

[24] Z. Wang, A. C. Bovik, H. R. Sheikh, and E. P. Simoncelli, "Image quality assessment: From error visibility to structural similarity," *IEEE Trans. Image Process.*, vol. 13, no. 4, pp. 600–612, Apr. 2004.

[25] K. Belkebir and M. Saillard, "Special section: Testing inversion algorithms against experimental data," *Inverse Problems*, vol. 17, no. 6, pp. 1565–1571, Dec. 2001.

[26] K. Belkebir and M. Saillard, "Testing inversion algorithms against experimental data: Inhomogeneous targets," *Inverse Problems*, vol. 21, no. 6, pp. S1–S3, Dec. 2004.

[27] J.-M. Geffrin, P. Sabouroux, and C. Eyraud, "Free space experimental scattering database continuation: Experimental set-up and measurement precision," *Inverse Problems*, vol. 21, no. 6, pp. S117–S130, Dec. 2005.

Martina Teresa Bevacqua (Member, IEEE) received the M.S. Laurea degree (summa cum laude) in electronic engineering and the Ph.D. degree in information engineering from the Mediterranea University of Reggio Calabria, Reggio Calabria, Italy, in July 2012 and May 2016, respectively.

She is currently an Associate Professor with the Mediterranea University of Reggio Calabria. Her research activity mainly concerns electromagnetic inverse problems, with particular interest in: 1) inverse scattering problems from both a theoretical and applicative point of view; and 2) field intensity shaping in nonhomogeneous and unknown scenarios for hyperthermia treatment planning, wireless power transfer, and MRI shimming.

Dr. Bevacqua was a recipient of the Barzilai Award from the Italian Electromagnetics Society in 2014 and the Young Scientist Award during the 2018 URSI Atlantic Radio Science Meeting. Moreover, she received the Honorable Mention from IEEE-Antennas and Propagation Society (Central and Southern Italy Chapter) in the 2016 Best Student Member Paper Competition. She was also a recipient of the Mojgan Daneshmand Grants by the Antennas and Propagation Society (APS-URSI 2023) and again the Young Scientist Award by the International Union of Radio Science (EMTS 2023). Moreover, in November 2023, she received the "2023 IEEE Antennas and Propagation Ulrich L. Rohde Best Innovative Conference Paper Awards on Antennas Measurements and Applications" during the 2023 IEEE International Conference on Antenna Measurements and Applications. Since April 2023, she has been the Vice-Chair of the IEEE Young Professional Affinity Group of the IEEE Italy Section.

Tommaso Isernia (Fellow, IEEE) received the Laurea (summa cum laude) and Ph.D. degrees from the University of Naples Federico II, Naples, Italy, in 1988 and 1992, respectively.

He is currently a Full Professor of electromagnetic fields with the Mediterranea University of Reggio Calabria, Reggio Calabria, Italy, where from 2018 to 2022, he was the Head of the Dipartimento di ingegneria dell'Informazione, delle Infrastrutture e dell'Energia Sostenibile (DIIES). He has founded and actually leads the Laboratory for ElectroMagnetic Methods and Applications (LEMMA) Group, DIIES. Under his direction, and also by virtue of the LEMMA Group Research Products, DIIES has been elevated to the grade of "Dipartimento di Eccellenza" by the Italian Ministry for Research. His current research interests include inverse problems in electromagnetics, with particular emphasis on phase retrieval, inverse scattering, and inverse source problems, as well as their applications to antenna synthesis, inverse design of innovative devices, and e.m. fields shaping for biomedical therapeutic applications.

Prof. Isernia was a recipient of the G. Barzilai Award from the Italian Electromagnetics Society in 1994.

Open Access funding provided by 'Univ Mediterranea di Reggio Calabria' within the CRUI CARE Agreement